Anal Bioanal Chem (2010) 396:899–910
DOI 10.1007/s00216-009-3269-8

ORIGINAL PAPER

Performance evaluation of mapping and linear imaging FTIR microspectroscopy for the characterisation of paint cross sections

Edith Joseph · Silvia Prati · Giorgia Sciutto · Marcella Ioele · Paola Santopadre · Rocco Mazzeo

Received: 10 September 2009 / Revised: 24 October 2009 / Accepted: 25 October 2009 / Published online: 12 November 2009

Abstract Different Fourier transform infrared microspectroscopic techniques, using attenuated total reflection (ATR) mode and single-element mercury–cadmium–telluride (MCT) detector (mapping) or multielement MCT detector (raster scanning), are compared with each other for the characterisation of inorganic compounds and organic substances in paint cross sections. All measurements have been performed on paint cross sections embedded in potassium bromide, a transparent salt in the mid-infrared region, in order to better identify the organic materials without the interference of the usual embedding resin. The limitations and advantages of the different techniques are presented in terms of spatial resolution, data quality and chemical information achieved. For all techniques, the chemical information obtained is found to be nearly identical. However, ATR mapping performed with a recently developed instrumentation shows the best results in terms of spectral quality and spatial resolution. In fact, thin organic layers (~10 μm) have been not only identified but also accurately located. This paper also highlights the recent introduction of multielement detectors, which may represent a good compromise between mapping and imaging systems.

E. Joseph · S. Prati · G. Sciutto · R. Mazzeo (✉)
Microchemistry and Microscopy Art Diagnostic Laboratory,
University of Bologna,
via Guaccimanni 42,
48100 Ravenna, Italy
e-mail: rocco.mazzeo@unibo.it

M. Ioele · P. Santopadre
Istituto Superiore per la Conservazione e il Restauro,
Piazza San Francesco di Paola 9,
00184 Rome, Italy

Keywords Fourier transform infrared (FTIR) microscopy · Attenuated total reflection (ATR) · Mapping · Linear imaging · Painting materials

Introduction

A sample collected from a painting shows a complex multilayered structure composed by mixtures of organic and inorganic substances depending on the type of support and execution technique adopted. The material characterisation of these multilayers structures is difficult to accomplish as the original paint layers' components may have been submitted to the deterioration processes and it may be difficult to be physically separate the layers due to their thickness (1–200 μm). Moreover, within a single paint layer, an uneven distribution of pigment and binding medium may occur. In both performing technical studies aimed at contributing to attribution studies or informing painting conservators on appropriate conservation measures, the need to spatially locate the different components within the typical multilayered structures represents an issue of great importance. In fact, it is know that the material constituents of repainted areas on ancient paintings differ from the constituents of the original painting. To this purpose, a deep understanding of the painting components as well as their ongoing degradation and ageing phenomena is required and can be achieved with the use of advanced analytical techniques working at morphological (optical microscopy), elemental (scanning electron microscopy–energy-dispersive X ray spectrometry and X-ray fluorescence microscopy) and molecular (Fourier transform infrared (FTIR) and Raman microscopies, secondary ion mass spectrometry, microspectrofluorimetry) levels [1–5].

FTIR microscopy, in particular, has been widely applied to the characterisation of painting materials thanks to its contemporary capability to characterise stratigraphically both inorganic and organic compounds [6–11]. The actual sample preparation procedure foresees the paint fragment to be embedded into a resin and cross-sectioned. Polyester resins are commonly used thanks to the fact that they are colourless, which allows the sample to be seen through and show almost no shrinkage after setting. They cure at room temperature and are easy to be sectioned, grinded and polished in order to reach the desired planarity of the paint stratigraphy to be analysed. Once properly prepared, paint cross sections can be analysed with different modalities.

Using a single-element detector in transmission or reflection mode, the spatial resolution is related to an adjustable aperture which cannot be lower than 10× 10 μm^2 in order to allow a sufficient radiation throughput and avoid diffraction effects. Improvement in the spatial resolution and in the spectral quality can be achieved by coupling the FTIR microscope with a synchrotron (SR) source [12, 13]. Improved spatial resolution and spectral quality can also be achieved by using attenuated total reflection (ATR) mode, which makes use of an internal reflection element (IRE) to analyse the surface of optically less dense materials placed in close contact with it. It is generally considered to be the most appropriate method for analysing cross sections thanks to the fact that the recorded spectra present similar features to those collected in transmission mode [14]. Thanks to the magnification factor of the IRE, the ATR configuration allows smaller areas to be investigated if compared with reflection or transmission mode [15, 16]. In fact, the dimension of the investigated area in a microscope can be estimated with the Rayleigh criterion: $d = 1.22\lambda/n_1 \sin\theta$ where d is the spatial resolution; λ is the wavelength; n_1 is the refractive index of the medium in which the measurement is conducted (i.e., the IRE or crystal), and θ is the most extreme ray entering the objective [17]. A clear advantage is that by maintaining a good spectral quality a better spatial resolution can be achieved. A drawback of the method is that a uniform contact between the sample and the ATR crystal is needed, which implies an accurate surface preparation [15, 18].

Apart from single-point analysis, the use of a motorised stage and/or multielement detectors has facilitated large data collection [19]. The introduction of mapping, imaging and raster scanning equipments allowed the collection of a large number of FTIR spectra from a surface and the elaboration of distribution maps of the identified compounds. On selected paint cross-sectional surface areas, specific spectral information can thus be obtained as distribution plots using the intensities of characteristic absorption bands against their spatial position [20, 21].

FTIR mapping systems perform sequential data collection, making use of a single-element mercury–cadmium–telluride (MCT) detector, adjustable apertures to select the investigated area and a motorised stage. The spatial resolution down to ~5 μm is here related to the aperture dimensions and to the acquisition method (reflection, transmission or ATR) as mentioned above. Furthermore, the overlapping between two adjacent surface areas during data collection allows further increase in the spatial resolution [21–23]. The main drawback of the mapping system is the acquisition time required, which is of the order of hours, which may, however, not be relevant when dealing within rare cultural heritage samples.

FTIR imaging consists of a simultaneous and therefore faster data collection, which makes use of a multichannel detector where small pixels of about 6 μm are distributed over a grid pattern (focal plane array, FPA) [24–26]. If compared with mapping, which makes use of geometrical apertures, the spatial resolution is here determined by the pixel dimension, but unfortunately this also means a poor spectral quality (low signal-to-noise ratio, S/N). In fact, the photon quantity received by each pixel is inversely proportional to the number of pixels, and for large detectors this means low photon quantity. The ATR configuration can provide increased spatial resolution of approximately 5 μm compared to transmission or reflection imaging [27–29]. The high spatial resolution achieved with this configuration is in fact competitive with the use of synchrotron radiation source which is a beam with a high brightness [30]. The cutoff of the focal plane array detector at 900 cm^{-1} represents a serious drawback when dealing with heritage materials as the distinction between salts belonging to the same class category (i.e. carbonates) is not possible. This happens, for example, with white chalk $CaCO_3$ and lead white $Pb(OH)_2{\cdot}PbCO_3$, two painting materials which show distinctive features down to 900 cm^{-1}.

The last decade has seen a great development of FTIR imaging with FPA detectors which became popular in various application fields, wherein particular dynamic processes are investigated [22, 31]. In spite of that, this technique is costly and still needs for special authorisation as these detectors have been historically used in military and space imaging application. Moreover, a delamination of the infrared-sensitive material which composes the FPA detector may occur and result in non-responsive pixels, contributing to its low lifetime [32].

More recently, linear array detectors (raster scanning) have been developed, combining together several MCT detectors and a motorised stage to perform sequential scan lines. This system has an acquisition time reduced by a factor corresponding to the number of detector elements. The individual elements are 25 μm in size and thus allow obtaining spectra with a good spectral quality [19, 33]. In

transmission or reflection mode, the achieved resolution of 25 μm can be reduced to 6.25 μm using optical zoom. In ATR mode, the spatial resolution is ~6 μm when a germanium crystal is used as IRE.

This paper aims to compare the performances of different micro-FTIR configurations for the characterisation of paint cross sections. In particular, ATR mapping and raster scanning have been tested and compared. To this purpose, an alternative embedding system which makes use of potassium bromide has been developed with the purpose of avoiding the interference caused by the embedding resin in the interpretation of the collected FTIR spectra [14, 34].

Experimental section

Samples Two paint fragments have been collected from the blue angel's wing (sample MCR13) of Mattia della Robbia's terracotta altarpiece "Assumption of Virgin between S. Sebastian and S. Rocco" (1527–1532 A.D.) located in the collegiate church of S. Maria Assunta in Montecassiano (Macerata, Italy) and from the angel's halo of the Giotto's Universal Judgement (sample 3 L) frescoes (1305 A.D.) located in the Scrovegni Chapel (Padua, Italy).

The selection of the two samples has been carefully made as they address specific painting conservation issues such as the characterisation of organic binding materials usually present in low concentration and dispersed in the inorganic matrix made up of pigments and ground preparation layers. In fact, inorganic materials are strongly absorbant in the mid-infrared region which results in the difficulty to detect absorbance bands specific to organic compounds. Furthermore, the characterisation of thin organic layers, which are at the limit of the theoretical spatial resolution of the instrumentation, represents a challenging issue. To this regard, both paint samples are characterised by the presence of gilding mordant layers mainly composed of organic materials, whose thickness is lower than 10 μm.

The sample preparation procedure is different according to the type of FTIR measurements to be performed afterwards. A possible approach is to perform specular reflection measurements directly on the surface of the cross section without any contact [15]. However, micro-irregularities present onto the surface result in spectra which are difficult to be interpreted because of the simultaneous presence of specular and diffuse reflection. In order to obtain a highly reflecting surface, a perfect sample planarity has to be achieved by using adequate and strenuous mechanical polishing methods [35], costly advanced techniques such as ion milling system, focused ion beam [36, 37] or ultramicrotomy [30, 38]. As a consequence, very few publications have been so far reported concerning the study of paint cross sections by FTIR microscopy in specular reflection mode [30, 38–40]. Analyses carried out in transmission mode offer a good spectral quality, but the multilayered paint sample has to be prepared as thin section (less than 15 μm thick) which is hard to be obtained. Alternative sample preparations foresee the paint fragment to be embedded in KBr and then polished from both sides until a thin slide is produced. This procedure results rather destructive for the fragment, as most of its constituents can be lost during polishing [34]. A thin section can also be obtained through the embedding of the sample in a polymer resin and then microtoming it in order to be submitted to transmission analyses [9, 41]. The paint fragment can also be directly squeezed into a diamond compression cell and then submitted to transmission analyses. This is a way to avoid the contamination effect produced to the spectra by the embedding resin [34, 42]. ATR measurements can be easily performed on cross sections, aside from the fact that a uniform contact between the sample and the ATR crystal is achieved. However, in order to obtain a good spectral quality, a microscopically flat area can be easily found with micro-ATR crystals [15]. In this paper, we will present ATR measurements, which have been performed on cross sections embedded in potassium bromide in order to avoid the interference of the absorbance bands of the embedding resin in the FTIR spectra.

After careful observation under a binocular stereo microscope Leica MZ6, the paint fragments have been cross-sectioned in potassium bromide (KBr) following an already published procedure which foresees the following steps [14]: first, 300 mg of KBr is pressed into a pellet under low pressure (2 tons for 30 s) in order to achieve a soft base where the paint fragment will be transferred which is then positioned with its surface parallel to the base and, afterwards, another 300 mg of KBr is added on. After a second low-pressure application (3 tons for 2 min), the pellet (13×2 mm) is carefully extracted and partially inserted in a polyester resin support in order to be more easily handled (Fig. 1) and better submitted to ATR measurements. Finally, the cross section is obtained through a careful dry polishing on aluminium oxide Micro-Mesh® papers with different grinding of 2,400, 4,000, 6,000, 8,000 and 12,000. This sequence allows a smooth surface to be achieved. The cross sections are then first submitted to optical microscope observations in order to document the stratigraphic morphology of the paint layers which are then chemically characterised by scanning electron microscopy coupled to energy-dispersive X-ray microprobe analysis (SEM–EDS). Afterwards, the cross sections are examined by different FTIR microscopy systems equipped with a conventional source and either single-element or multi-channel detectors.

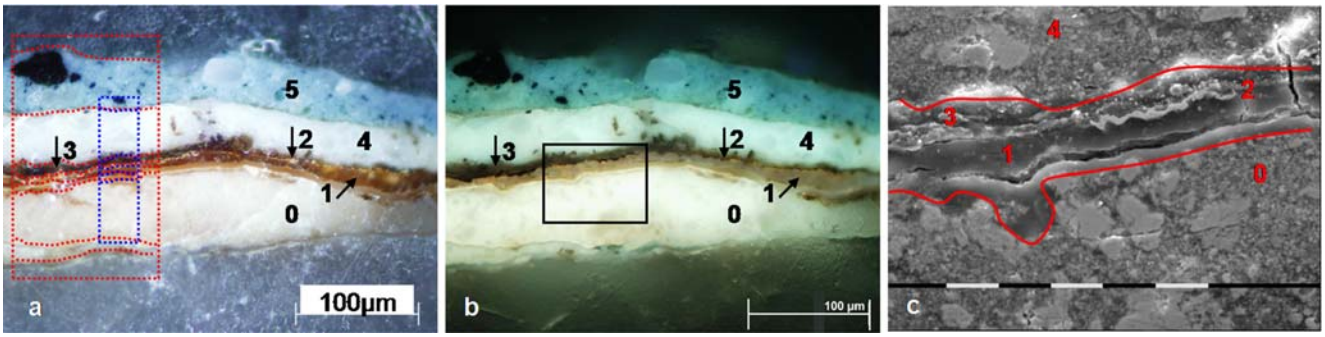

Fig. 1 Cross section photomicrographs of sample MCR13 embedded in KBr: **a** visible light microscopic image; **b** UV light microscopic image: the *black box* indicated the selected area for the SEM–EDX analysis; **c** secondary electron image (original magnification ×1,600): the detachment occurring between the white ground layer (*0*) and the gold leaf (*2*) is visible

Optical microscopy Dark field observations have been performed using an optical microscope Olympus BX51M equipped with fixed oculars of ×10 and objectives with different magnifications (×5, ×10, ×20, ×50 and ×100). Visible and ultraviolet light have been respectively provided by a 100-W halogen projection lamp and an Ushio Electric USH102D lamp. Cross-sectional photomicrographs have been recorded with a digital scanner camera Olympus DP70 directly connected to the microscope.

Scanning electron microscopy A scanning electron microscope, Philips XL 20 model SEM–EDX equipped with an energy-dispersive X-ray analyser, was used to analyse the cross sections, which have previously been sputtered with carbon. It is worth saying that such technique has been performed after the FTIR measurements as the stratigraphy of the cross section can be slightly modified in case of re-polishing for further analyses to be performed afterwards. The elemental composition of the different paint layers was performed with an acceleration voltage of 25–30 keV, lifetime >50 s, CPS≈2,000 and working distance 34 mm. EDX-4 software equipped with a ZAF correction procedure for bulk specimens was used for semi-quantitative analyses of the X-ray intensities.

FTIR microscopy

ATR mapping with single-element detector

1. A Thermo-Nicolet Nexus 5700 spectrometer coupled with a Nicolet Continuμm FTIR microscope fitted with an MCT detector cooled by liquid nitrogen and a ×15 Thermo-Electron Infinity Reflachromat objective with a tube factor of ×10 has been used. ATR spectra have been acquired in the range 4,000–650 cm^{-1}, at a spectral resolution of 4 cm^{-1}, using a slide-on ATR objective with a hemispherical silicon crystal. A background single-beam spectrum of the clean ATR crystal has been first collected with the slide-on ATR objective inserted but not in contact with the sample surface. A total of 64 scans have been recorded and the resulting interferogram averaged. For the ATR mapping on a selected area (120×230 μm^2 for sample MCR13), a step size of 20 μm in x-direction and 10 μm in y-direction has been chosen with an aperture of 100×100 μm, relative to an investigated area of ~29×29 μm^2. For sample 3 L, which contains a very thin organic layer of the order of 3–5 μm, a line map has been achieved with a step size of 5 μm in y-direction and an aperture of 150×50 μm, relative to an investigated area of ~44×15 μm^2. Once a spatially related series of spectra have been acquired, a data processing method, using Nicolet OMNIC Atlμs™ software, treats the set of spectra collectively, i.e. the whole data set was baseline-corrected rather than each spectrum having to be processed individually. Then, specific chemical absorption bands of the compound under investigation were selected and their areas, defined as an interval of 20 cm^{-1} centred on the maximum of the absorbance signal, plotted against the spatial position of each spectrum in the series. This approach allowed information on the spatial distribution of the identified chemical compounds. Each false-colour image obtained from the map data set results from the area of one specific chemical vibration band (chemical map) plotted against the spatial position of each spectrum in the data set. A colour scale from high value (red) to low value (blue) is employed.
2. A Nicolet iN™10MX imaging microscope, fitted with an MCT detector cooled by liquid nitrogen, has also been used in order to perform ATR mapping. If compared with the previous equipment, where the infrared beam generated by the FTIR spectrometer has to be directed to the microscope through an external port, the iN™10MX microscope integrates the interfer-

ometer, source, laser and detector into a single compartment, which allow a high-energy output and a very high S/N ratio. FTIR spectra can also be collected at ambient temperature with a deuterated triglycine sulphate (DTGS) detector. The measurements have been performed using a slide-on ATR objective with a conical germanium crystal, in the range 4,000–680 cm^{-1}, at a spectral resolution of 4 cm^{-1} and with 16 scans. Backgrounds have been first acquired with the slide-on ATR objective inserted but not in contact with the sample surface. The selected areas (30×120 μm^2 for sample MCR13 and 36×126 μm^2 for sample 3 L) have been analysed with a step size of 5 μm (3 μm for sample 3 L) and an aperture of 20×20 μm resulting in an investigated area of 5×5 μm^2. The data processing method used is similar to that of the Continuμm FTIR microscope and makes use of a dedicated OMNIC Picta™ software.

ATR raster scanning with linear array detector

A Nicolet iN™10MX imaging microscope, fitted with a 16-element MCT detector array cooled by liquid nitrogen, has been used with a slide-on ATR objective equipped with a conical germanium crystal. In this configuration, the spatial resolution is 6.25 μm. ATR measurements have been performed on selected areas (225×130 μm^2 for sample MCR13 and 206×150 μm^2 for sample 3 L) with eight and two scans, respectively, at a spectral resolution of 4 cm^{-1} in the range 4,000–720 cm^{-1}. A background single-beam spectrum of the clean ATR crystal has been first collected with the slide-on ATR objective inserted but not in contact with the sample surface.

The spatial resolution and spectral range setup used are summarised in Table 1.

Results and discussion

Characterisation of thin organic layer based on proteinaceous material and paint layers made up of mixture of inorganic and organic compounds (sample MCR13) by the use of conventional ATR mapping with single-element detector

The optical microscope observation of the sample cross section MCR13 (Fig. 1a) highlights its multi-layered structure. In fact, a light blue paint layer (layer 5, 20–50 μm thick), composed of a mixture of white and few blue pigment particles and a completely white one (layer 4, 30 μm thick) are superimposed to a gold leaf (layer 2), under which a brownish gilding mordant (layer 1, 4–14 μm thick) and a white layer (layer 0, 20–60 μm thick) are visible. A thin dark layer (layer 3, 5–10 μm thick), which is probably due to deposition materials, can also be observed over the gold leaf and suggests that the angel's wing was originally gilt and later on repainted with a light blue paint layer. Furthermore, a detachment visible between the organic mordant (layer 1) and the lower white paint layer 0 can be observed and better highlighted by SEM (Fig. 1c) and optical microscope observation under UV light illumination (Fig. 1b) that also shows how both layers 0 and 4 are characterised by a strong bright yellow fluorescence while the gilding mordant fluoresces just pale blue (Fig. 1b). It is worth mentioning how the use of the KBr embedding system greatly improves the microscopic documentation of the fluorescence generated by paint layers as the interference with the fluorescence phenomena generated by the commonly used embedding resin systems are in this case avoided.

Micro-ATR mapping measurements (Fig. 2) have been carried out on a representative area of the sample (120×230 μm^2) indicated with a red box in Fig. 1a. By integrating the CO_3^{2-} in-plane bending band at 679 cm^{-1} (Fig. 2a), the presence of lead white pigment (basic lead carbonate $2PbCO_3 \cdot Pb(OH)_2$) has been localised in the white layers 0 and 4 and in the light blue layer 5. In particular, layer 0 is enriched in cerussite (lead carbonate) as it can be appreciated by integrating the CO_3^{2-} out-of-plane bending band at 839 cm^{-1} (Fig. 2b). Lead white is a well-known synthetic pigment that, according to different recipes, can be characterised by different relative amount of hydrocerrusite and cerussite [43]. The differences found in the composition of the lead white based layers could indicate the use of pigments from different manufacturers, even though the transformation of hydrocerrusite into cerussite (or the reverse), due to weathering conditions, cannot be excluded [44]. It has not been possible to characterise the fine dark blue particles which are mixed to lead white in layer 5 (Fig. 1a). This is probably due to both their low concentration and very small size which are under the detection and/or spatial resolution limits of the system used. Gypsum (SO_4^{2-} asymmetric stretching, 1,112 cm^{-1}) has been detected within both the dark layer 3 and the mordant layer 1 (Fig. 2c). Its presence within layer 3 can be linked to deposition material whereas its presence within the mordant layer 1 is hard to be explained. In fact, ancient gilding mordant techniques do not mention the use of gypsum and, therefore, a contamination from closer paint layers caused by the probably low spatial resolution of the system configuration used can be hypothesised, as will be discussed herewith after. On the other hand, the characterisation of the different binding media has been successfully achieved. In fact, by mapping the ester C=O stretching band at 1,732 cm^{-1} (Fig. 2d), the detection of a lipidic

Table 1 Technical characteristics of the different FTIR microscopic techniques and experimental conditions for samples MCR13 and 3 L

	Raster scanning iN™10MX	Mapping iN™10MX	Mapping Continuμm
Technical characteristics			
Spectral region investigated (cm^{-1})	4,000–720	4,000–675	4,000–650
Lower practical limit of aperture (μm^2)	–	20×20	50×50
Pixel dimension (μm)	25	–	–
S/N ratio	Very high	Very high	High
Investigated area (μm^2)	Multiple of 12×100	Variable	Variable
Detector lifetime	High	High	High
Acquisition time	2–30 min	min–h	h
Experimental conditions			
Aperture MCR13	–	20×20	100×100
Aperture 3 L	–	20×20	150×50
ATR crystal	Ge	Ge	Si
Step size (μm) MCR13	–	5	20-x, 10-y
Step size 3 L	–	3	5-y
Spectral resolution (cm^{-1})	4	4	4
Spatial resolution (μm)	6.25	5	10
Scans MCR13	8	16	64
Scans 3 L	2	16	64

Ge conical germanium, *Si* hemispherical silicon, *-x* x direction, *-y* y direction

binder has been obtained and its spatial distribution within both the repainted layers (layers 4 and 5) and the white ground (layer 0) located. By integrating the amide I absorbance band at 1,638 cm^{-1}, the detection of proteinaceous material has been achieved within both the thin mordant layer 1 and the thin dark layer 3 present over the gold leaf (Fig. 2e). In the first case, it can be attributed to a glue size gilding technique whereas its presence in layer 3 could be due to the application of a proteinaceous-based protective/finishing layer applied over the gold leaf. Ancient treatises mention for gilding either the use of a mixture of siccative oil and natural resins or a glue size mixed with red bole [45, 46]. However, as already mentioned above for gypsum, this could also be due to the fact that the dark layer and the mordant layer, whose thickness is lower than 10 μm, cannot be differentiated with this system.

Unfortunately calcium oxalates, which are known to be the result of organic binders' degradation phenomena and/or biological activity[46], show infrared bands in the same spectral region of the amide I, and therefore, the distribution plot carried out at 1,638 cm^{-1} cannot be considered a specific feature for the detection of protein binders. In fact, as shown in Fig. 2f, which has been obtained by integrating the characteristic oxalates O–C–O stretching band at 1,319 cm^{-1}, their presence has been also confirmed in

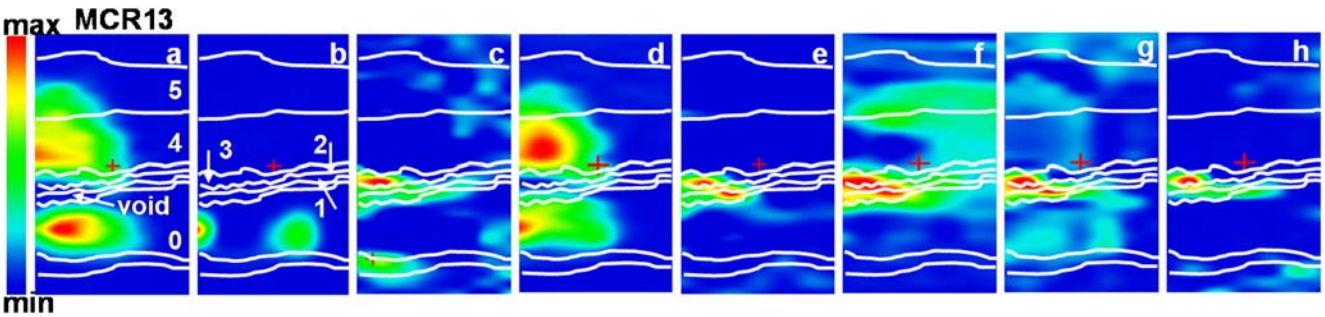

Fig. 2 ATR mapping continuum, sample MCR13: FTIR false-colour plots representing (*a*) lead white (peak area 679 cm^{-1}), (*b*) cerussite (peak area 839 cm^{-1}), (*c*) gypsum (peak area 1,112 cm^{-1}), (*d*) siccative oil (peak area 1,732 cm^{-1}), (*e*) amide I (peak area 1,638 cm^{-1}), (*f*) oxalates (peak area 1,319 cm^{-1}), (*g*) proteinaceous material (correlation map with a reference spectrum of glue) and (*h*) silicates (correlation map with a reference spectrum of bole)

layer 1, 3 and 4. At the same time, the amide II band (1,600–1,550 cm^{-1}) cannot be used as indicative of the presence of proteinaceous materials as this band overlaps with that typical of metal carboxylates which are produced through the interaction of pigments and binders. In spite of that, the presence of proteinaceous material has been confirmed in both layers 1 and 3, performing a correlation map with a reference spectrum of animal glue (Fig. 2g). The presence and spatial location of silicates has been performed, and the correlation map with a reference spectrum of red bole pigment (a natural ferruginous aluminium silicate red pigment) revealed their presence in both layers 1 and 3 (Fig. 2h). In the first case, their presence is certainly related with the ancient gilding technique whereas the presence of silicates in layer 3 could be correlated with deposition material. The presence of siccative oil as binder of the white ground layer 0 and the detection of a proteinaceous material used for gilding may explain the observed gold leaf detachment (Fig. 1c). Differences in their chemical composition may have given rise to different response to external physical stresses. It can be noticed that no signal has been acquired in the right part of the investigated area (Fig. 3) where the detachment has been observed. In fact, one of the main difficulties encountered when working in ATR with a hemispherical crystal is due to its non-perfect contact with non-perfectly planar surfaces which have not been carefully polished. To this regard, the preparation of paint cross sections embedded in KBr should be carefully performed by paying great attention to the application of a gentle and constant pressure during the polishing procedures.

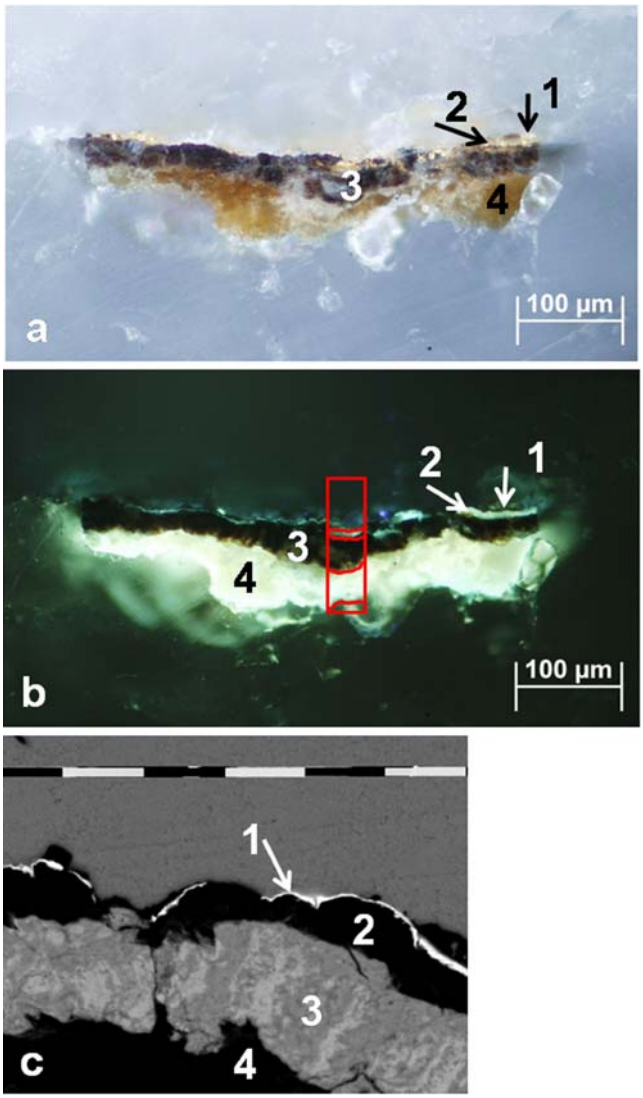

Fig. 3 Cross section of sample 3 L embedded in KBr: **a** visible light microscopic image: the red box indicated the selected area for the ATR mapping; **b** UV light microscopic image; **c** BSE image (original magnification ×1,300) of sample 22 L with a similar structure: the different layers are numbered from 1 to 4: gold leaf (*1*), gold mordant layer (*2*), tin leaf (*3*) and tin mordant layer (*4*)

Characterisation of oil-based thin organic layer (sample 3 L) by the use of conventional ATR mapping with single-element detector

In order to help interpret and complement the ATR–FTIR results, the 3 L cross section has been first observed under optical microscope. The visible and UV light images illustrated in Fig. 3 indicate that a golden tin technique has been adopted. Despite the fact that different definitions of "stagno dorato" (golden tin) are reported [47, 48], Giotto made use in this case of a fine real gold leaf superimposed to a tin foil instead of a tin foil tinted with a golden varnish which represented in the ancient techniques a cheap substitute for gold. A gold leaf (layer 1) has been applied over a tin leaf (layer 3) by the use of a thin mordant gilding (layer 2, 3–5 µm thick) which fluoresces bright yellow when observed under UV light (Fig. 3b). This feature is generally considered as a first indication of the presence of an oily substance. The tin foil itself was fixed to the wall by means of another mordant layer (layer 4, 15–50 µm thick), which also shows a bright yellow fluorescence when observed under UV illumination. The use of a golden tin technique has been confirmed by SEM–EDX elemental analyses. In fact, both tin and gold have been identified in the different metal leaves which appear, respectively, grey and white in the BSE image (Fig. 3c) [49–52].

ATR–FTIR mapping measurements performed on sample 3 L by the use of conventional ATR mapping with single-element detector have not been successful in the characterisation and spatial location of the very thin mordant layer 2. This can certainly be explained by the fact that the thickness of this thin layer is below the spatial resolution achievable with this configuration.

Characterisation of thin organic layer based on proteinaceous material and paint layers made up of mixture of inorganic and organic compounds (sample MCR13) by the use of ATR raster scanning with linear array detector on the iN™10MX microscope

A selected area (225×130 μm^2) of sample MCR13 has been submitted to ATR raster scanning (Fig. 4a). In this case, the spectra have been recorded in extreme conditions by using only eight scans but maintaining a high signal-to-noise ratio. Since this system allows the investigation of larger areas, it has also been possible to achieve a wide overview of the present compounds, which could not be detected by performing measurements on small areas. In fact, gypsum has been mainly identified and located in the thin dark layer 3 by imaging the SO_4^{-2} asymmetric stretching at 1,113 cm^{-1} (Fig. 4b). However, in correspondence to gold leaf discontinuities, gypsum has penetrated into the below thin organic layer 1 and its presence detected accordingly. As already mentioned, gypsum is often associated to deposition material and its presence in layer 3 confirms that the upper paint layers are not original and have been painted at a later stage. Given the fact that the 1,636 cm^{-1} band is not specific for oxalates as proteinaceous material absorb in the same spectral region, the O–C–O stretching absorbance at 1,320 cm^{-1} has been used as the characteristic band for oxalates (Fig. 4c). On the other hand, the binding medium used for gilding has been identified and exactly localised in the mordant layer 1 using a correlation map on the amide functional group (Fig. 4d). It is worth mentioning how the thickness measured (8 μm) in the infrared image for proteins is of the same order than the thickness (5–15 μm) of the mordant layer in the visible light image, indicating the high spatial resolution thus achieved with raster scanning. Moreover, the fine dark blue pigment particles of about 10 μm present in layer 5 have been identified as indigo, using one of its characteristic bands at 1,076 cm^{-1} (Fig. 4e). Indigo is a blue vegetable colouring matter that for use as a paint pigment is ground directly to a fine powder for mixture, as in this case, with lead white in order to obtain the desired light-blue tonality. Its detection may be difficult when mixed with highly absorbant inorganic pigments (lead white) and degradation products generated by aged binding media (siccative oils). In spite of that, its identification and spatial location have been achieved here thanks to the greater energy output and spatial resolution of this configuration (Fig. 5a, c). With respect to the ATR mapping extracted spectrum of the light blue layer 5 obtained with conventional microscopy (Fig. 5a), where no absorbance bands related to indigo are observed, the ATR raster scanning-extracted spectrum of the same layer shows some indigo characteristic absorbance bands at 1,076, 1,130, 1,198 and 1,629 cm^{-1}.

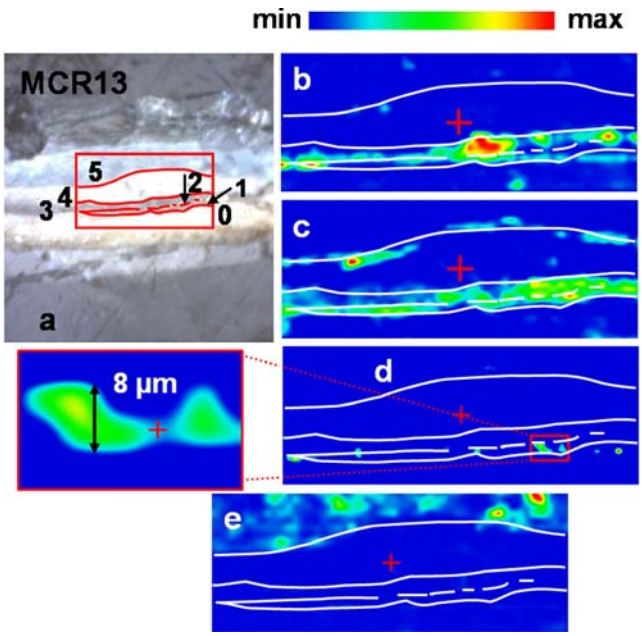

Fig. 4 (*a*) ATR raster scanning, sample MCR13: visible light FTIR microscopic image: the *box* indicated the selected area for the ATR raster scanning. FTIR false colours representing (*b*) gypsum (peak area 1,113 cm^{-1}), (*c*) oxalates (peak area 1,319 cm^{-1}), (*d*) amide correlation map with details of the layer thickness about 8 μm and (*e*) indigo (peak area 1,076 cm^{-1})

Characterisation of oil-based thin organic layer (sample 3 L) by the use of ATR raster scanning with linear array detector on the iN™10MX microscope

ATR–FTIR raster scanning has been performed directly on the 3 L cross section on a representative area (63×63 μm^2) marked with a red box in Fig. 6a. If compared with the unsuccessful results achieved with conventional ATR mapping, this system allowed the identification and localisation of the different inorganic and organic compounds constituting the paint layers. The distribution plot of the C–H aliphatic stretching absorbance bands between 2,990 and 2,830 cm^{-1} seems here to be localised within the tin mordant layer 4 and can only be related to the presence of organic substances (Fig. 6b) as the KBr embedding material is inactive within the mid-infrared region. In particular, a mixture of siccative oil and natural resin can be suggested thanks to the contemporary presence of the fatty ester band and the asymmetric stretching band of the carboxylic acid at 1,707 cm^{-1} (Fig. 6c). The assignment to a mixture of oil and natural resin is further confirmed by the existence of specific ancient recipes for mordant preparations [46–48, 53].

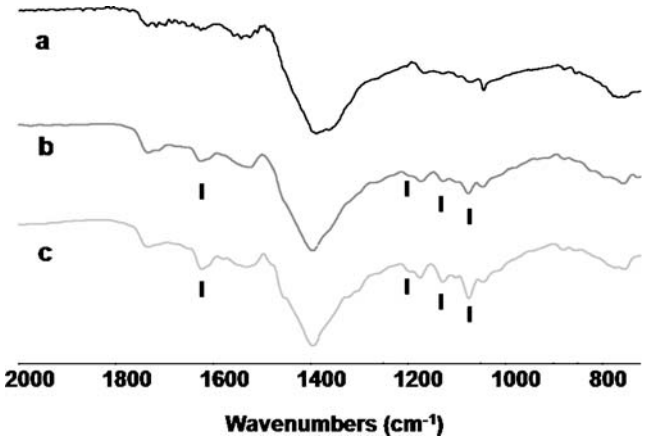

Fig. 5 (*a*) ATR mapping-extracted spectrum obtained from the layer 5 of sample MCR13 with conventional microscopy, aperture 100× 100 μm (investigated area of ~29×29 μm^2) and 64 scans. (*b*) ATR mapping-extracted spectrum obtained from the same layer with the integrated FTIR microscope, 20×20 μm (investigated area of 15× 15 μm^2) and 16 scans and (*c*) ATR raster scanning-extracted spectrum obtained from the same layer with integrated FTIR microscope and eight scans

Calcium oxalates are located within the tin mordant layer 4, and their mapping was achieved by integrating the O–C–O stretching band at 1,319 cm^{-1}. Moreover, they seem to be also present within a region close to the gold mordant layer 2 (Fig. 6d). The pixel dimension of this type of detector allows us to reach a high spatial resolution of approximately 6.25 μm. However, this is not enough to accurately image the very thin gold mordant layer 2 which has a lower than 5-μm thickness.

ATR mapping with single-element detector on the iN™10MX microscope

The presence of the infrared source directly located inside the FTIR microscope allows the avoidance of loss of energy due to the shorter optical path. For this reason, it is possible to reduce both the aperture, which in turn improves the spatial resolution and the number of scans, which decreases the time of analysis. As illustrated in Fig. 7, single-point ATR measurements performed on the white paint layer 0 of sample MCR13 using lower aperture (60×60 μm) than the ones used with conventional microscopy (100×100 μm) resulted in the spectral quality to be maintained, even with lower numbers of scans (32 instead of 64). In the same way, as illustrated in Fig. 8, the analysis of the same area of 6.25×6.25 μm by ATR mapping requires an aperture of 25 μm whereas with conventional FTIR microscopy this setting would not allow us to record any spectra.

Proteinaceous-material-based thin organic layer and mixture of inorganic and organic compounds (sample MCR13)

ATR mapping measurements have been performed on the same MCR13 cross section by adopting even more extreme parameter setup, which is a reduction to 20×20 μm aperture and number of scans to 16 with the aim of better characterising the thin organic layers 1 and 3. The chemical maps obtained (Fig. 9) from an area of 30×120 μm^2 (blue box in Fig. 2a) are rather consistent with the results obtained with the Continuμm FTIR microscope and the

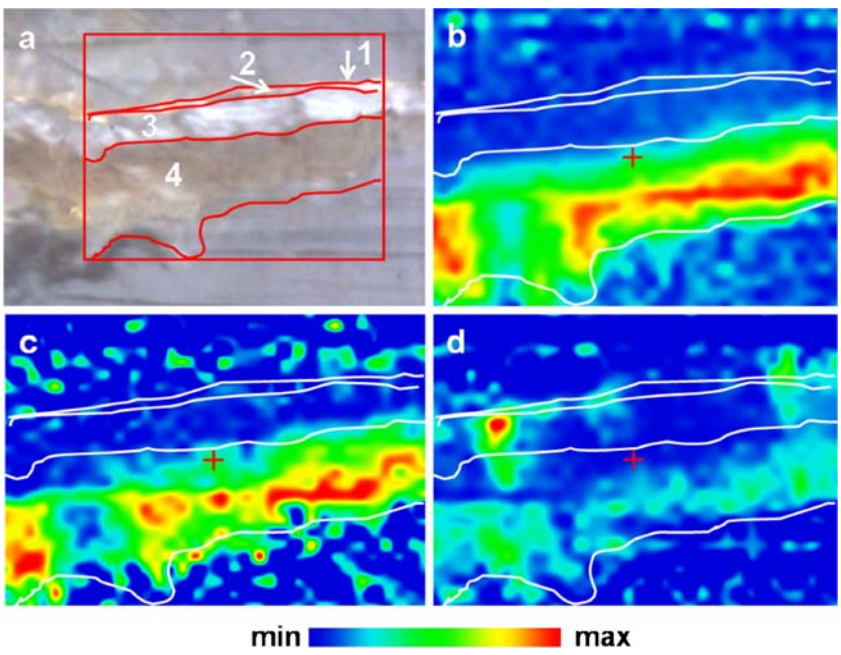

Fig. 6 **a** ATR raster scanning, sample 3 L: visible light FTIR microscopic image: the *box* indicated the selected area for the ATR raster scanning. FTIR false colours representing **b** aliphatic CH (region of interest 2,990–2,830 cm^{-1}), **c** fatty acids (peak area 1,707 cm^{-1}) and **d** oxalates (peak area 1,320 cm^{-1})

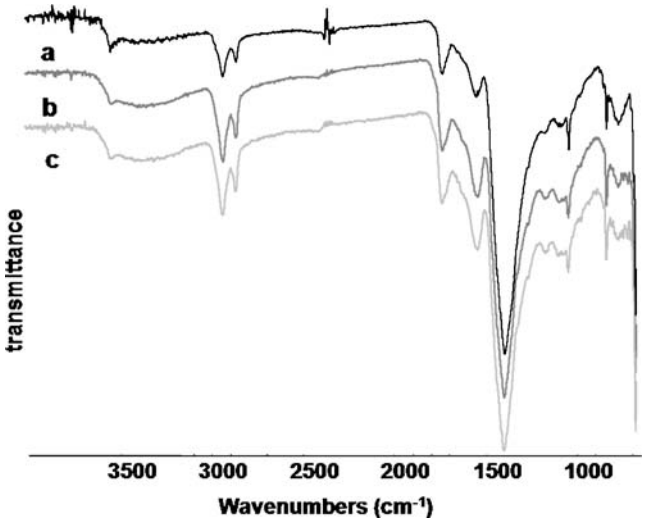

Fig. 7 (*a*) ATR spectrum obtained from the layer 0 of sample MCR13 with conventional microscopy, aperture 100×100 μm (investigated area of ~29×29 μm^2) and 64 scans. (*b*) ATR spectrum obtained from the same layer with integrated microscopy, 60×60 μm (investigated area of 15×15 μm^2) and 64 scans and (*c*) the same point but with 32 scans

raster scanning configuration. Gypsum (SO_4^{2-} stretching, 1,111 cm^{-1}) has been better identified as a deposition material and precisely localised as constituent of the thin dark layer 3 (Fig. 9a). Moreover, the location of proteinaceous material has been accurately assigned to the thin mordant layer 1 using a correlation map with a reference spectrum of animal glue (Fig. 9b). The elaboration of a correlation map with red bole pigment spectrum resulted in a localization which correspond to that of the proteinaceous material previously mentioned (Fig. 9c). If compared with the ATR mapping performed with conventional FTIR microscope, the chemical information obtained is substantially the same, but the chemical maps are more accurate, thanks to the improved spatial resolution and, in particular, the presence of proteinaceous material, and silicates are confined within the thin mordant layer, while gypsum appears as deposition material in the above dark layer. In addition, the fine blue pigment present within layer 5, which could not be previously identified with conventional FTIR microscope, turned out to be indigo (1,076 cm^{-1}; Fig. 9d). The great energy output and spatial resolution of this configuration are comparable to raster scanning, and the identification and spatial location of an organic pigment present in very small quantity have been achieved here (Fig. 5a, b). As illustrated above for raster scanning, the indigo characteristic absorbance bands at 1,076, 1,130, 1,198 and 1,629 cm^{-1} are observed on the ATR mapping extracted spectrum obtained with the integrated FTIR microscope (Fig. 5b) whereas no indigo is detected with conventional microscopy (Fig. 5a). Chemical maps of the other identified compounds (lead white, cerussite, oxalates and siccative oil) are similar to those obtained with conventional FTIR microscope (Fig. 9e–h).

Oil-based thin organic layer (sample 3 L)

ATR–FTIR mapping has been performed directly on the KBr cross section on a representative area (36×126 μm^2) marked with a red box in Fig. 3b. As illustrated in Fig. 10a, the resulting image obtained plots the intensity of the CH aliphatic stretching absorbance bands between 2,990 and 2,830 cm^{-1} and has allowed the localising of the different organic substances. The distribution plot of the acid C=O asymmetric stretching band at 1,707 cm^{-1} (Fig. 10b) and the FTIR spectra extracted from the different areas have suggested the presence of a mixture of siccative oil with natural resin in both the gold mordant and tin mordant layers (layers 2 and 4 respectively). Calcium oxalates, which may be derived from organic compounds' degradation, have been also identified in the different organic layers integrating the O–C–O stretching band at 1,320 cm^{-1} (Fig. 10c). The distribution of carboxylates as degradation products has been also plotted using the integrated asymmetric COO^- stretching absorbance at approximately 1,555 cm^{-1} (Fig. 10d) and coincided with the inner tin mordant layer. With respect to ATR microscopic conventional mapping, where no results have been achieved, and raster scanning systems, where lower spatial resolution is available, the thin mordant layer of 5 μm has been determined here. In fact, as the optical path length between source and objective is reduced, the integrated system iN10X benefits from higher energy output and permits working with lower apertures (20×20 μm^2), which there-

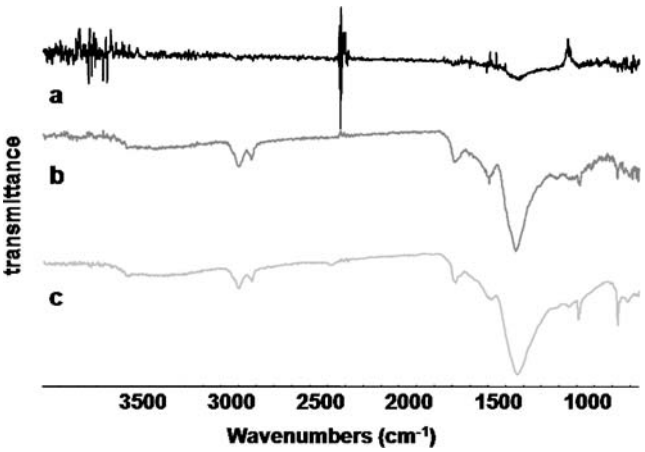

Fig. 8 (*a*) ATR spectrum obtained from the layer 0 of sample MCR13 with conventional microscopy, aperture 25×25 μm and 64 scans. (*b*) ATR spectrum obtained from the same layer with integrated microscopy, 25×25 μm and 64 scans and (*c*) ATR spectrum obtained from the same layer with integrated microscopy and raster scanning detector

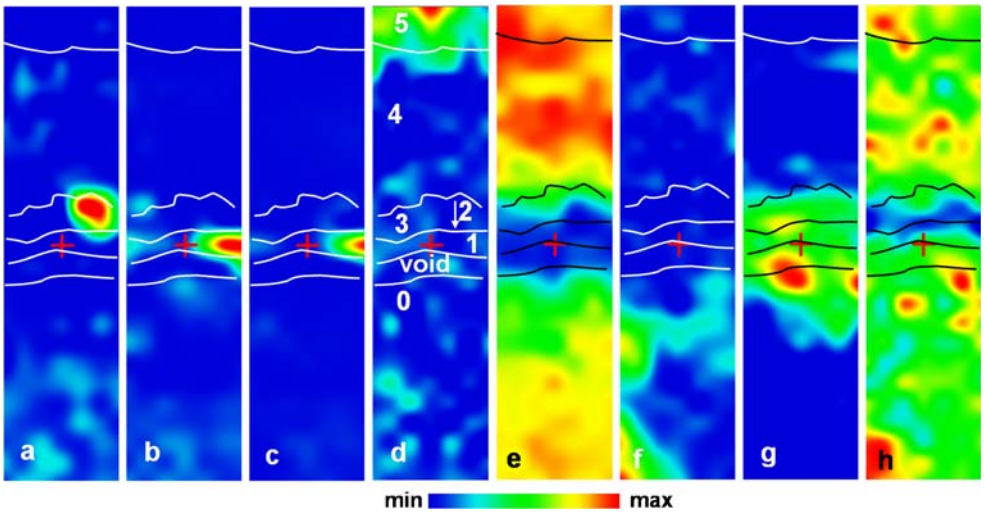

Fig. 9 ATR mapping-iN™-10MX, sample MCR13: FTIR false-colour plots representing (*a*) gypsum (peak area 1,111 cm^{-1}), (*b*) proteinaceous material (correlation map with a reference spectrum of glue), (*c*) silicates (correlation map with a reference spectrum of bole) and (*d*) indigo (peak area 1,076 cm^{-1})

fore results in a better spatial resolution. High-quality FTIR spectra are also obtained with a high signal-to-noise ratio or with a reduced acquisition time (16 scans).

Conclusions

In this paper, FTIR mapping with a conventional DTGS detector is compared in terms of chemical information, data quality and accurate spatial localisation with FTIR mapping with a recently developed integrated system and raster scanning in ATR mode. The different technical characteristics of each method used in this article are reported below in Table 1. ATR mapping and raster scanning with the integrated system provide better S/N ratios with shorter acquisition time with respect to the conventional ATR mapping system. These features are particularly important for the identification and spatial location of thin organic layers within the paint cross sections or of organic materials mixed in low quantity with other organic and inorganic materials.

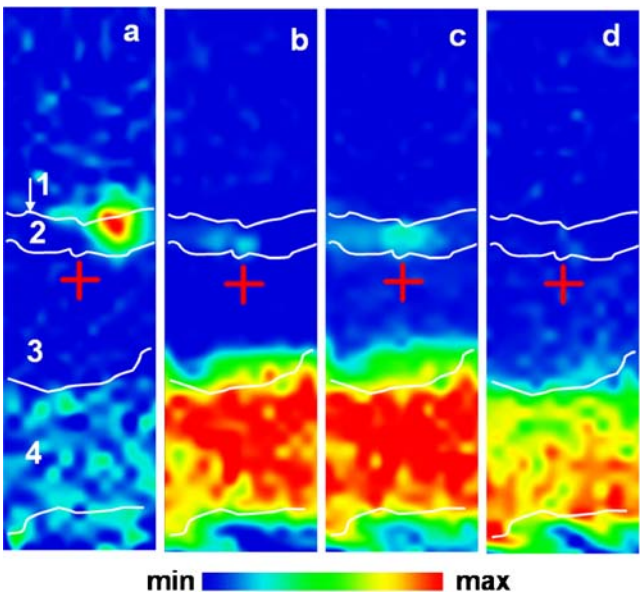

Fig. 10 ATR mapping- iN™10MX, sample 3 L: FTIR false-colour plots representing **a** aliphatic CH (region of interest 2,990–2,830 cm^{-1}), **b** fatty acids (peak area 1,707 cm^{-1}), **c** oxalates (peak area 1,320 cm^{-1}) and **d** carboxylates (peak area 1,555 cm^{-1})

With both setups, the characterisation of indigo in sample MCR13 was accomplished whereas it was not detected with the conventional system. Moreover, with the two setups, a better characterisation of the thin layers has been obtained. The 3 L sample shows how the mapping approach with the integrated system allows reaching spatial resolution down to 5 μm while raster scanning is not suitable for a clear distinction of the thinner mordant layer. This finding leads to the conclusion that the mapping performed with the integrated system shows here the best results with high spectral quality and spatial resolution.

However, raster scanning offers a fast and convenient method for the analysis of large sample areas with a high spatial resolution and a good data quality (minimum analysed area is 12×100 μm^2) in order to obtain a more statistical information about the homogeneity of the different layers. Given the larger spectral region (4,000–720 cm^{-1}) with respect to the FPA imaging systems, this technique presents straightforward advantages for the characterisation of paint cross sections.

In conclusion, the two methods can be used in a complementary way with mapping leading to the best spatial resolution and raster scanning to a more statistical product distribution. The spatial resolution

that the two systems are able to reach is extremely useful in the cultural heritage field and allows avoiding the employment of other approach in which the sample needs to be microtomed and/or analysed in transmission with SR radiation.

Acknowledgment This research has been partially carried out with the support of the European Union, within the VI Framework Programme (Contract: EU-ARTECH, RII3-CT-2004-506171). The authors also acknowledge the European Synchrotron Radiation Facility for providing synchrotron radiation facilities and would like to thank Dr. M. Cotte for assistance in using beamline ID21.

References

1. Matteini M, Moles A (2003) Scienza e restauro, Metodi di indagine. Nardini Editore, Florence
2. Pinna D, Galleotti M, Mazzeo R (2009) Scientific examination for the investigation of paintings: a handbook for conservators-restorers. CentroDi, Firenze
3. Cotte M, Welcomme E, Sol VA, Salom M, Menu M, Walter P, Susini J (2007) Anal Chem 79:6988–6994
4. Keune K, Boon JJ (2004) Anal Chem 76:1374–1385
5. Bottiroli G, Gallone A, Masala B (2005) Bollettino d'arte volume speciale (Giotto nella Cappella degli Scrovegni), pp 83–105
6. Van't Hul-Ehrnreich EH (1970) Stud Conserv 15:175–182
7. Baker MT, Von Endt DW (1988) Mater Issues Art Archaeol 123:71–76
8. Gillard RD, Hardman SM, Thomas RG, Watkinson DE (1994) Stud Conserv 39:187–192
9. Derrick MR, Stulik DC, Landry JM (1999) Infrared spectroscopy in conservation science. The Getty Conservation Institute, Los Angeles
10. Pilc J, White R (1995) Natl Gallery Tech Bull 16:73–84
11. Langley A, Burnstock A (1999) Proceedings of the 12th Triennial Meeting of ICOM Committee for Conservation. James & James, London
12. Reffner JA, Martoglio PA, Williams GP (1995) Rev Sci Instrum 66:1298–1302
13. Dumas P, Miller L (2003) Vib Spectrosc 32:3–21
14. Mazzeo R, Joseph E, Prati S, Millemaggi A (2007) Anal Chim Acta 599:107–117
15. Reffner JA, Martoglio PA (1995) In: Humecki HJ (ed) Practical guide to infrared microspectroscopy. Marcel Dekker, New York
16. Lewis LL, Sommer AJ (2000) Appl Spectrosc 54:324–330
17. Lewis LL, Sommer AJ (1999) Appl Spectrosc 53:375–380
18. Katon JE (1996) Micron 27:303–314
19. Bhargava R, Levin IW (2005) Spectrochemical analysis using infrared multichannel detector. Blackwell, Oxford
20. Treado PJ, Morris MD (1993) In: Morris MD (ed) Microscopic and spectroscopic imaging of the chemical state. Marcel Dekker, New York
21. Krishnan K, Powell JR, Hill SL (1995) In: Humecki HJ (ed) Practical guide to infrared microspectroscopy. Marcel Dekker, New York
22. Hartcock MA, Atkin SC (1988) In: Messerschmidt RG (ed) Infrared microspectroscopy. Theory and applications. Marcel Dekker, New York
23. Bhargava R, Wall BG, Koenig JL (2000) Appl Spectrosc 54:470–479
24. Ebizuka N, Wasaki M, Kobayashi Y, Sato S (1995) Appl Opt 34:7899–7906
25. Lewis EN, Treado PJ, Reeder RC, Story GM, Dowrey AE, Marco C, Levin IW (1995) Anal Chem 67:3377–3381
26. Burka EM, Curbelo R (2000) US patent 6141100
27. Chan KLA, Kazarian SG, Mavraki A, Williams DR (2005) Appl Spectrosc 59:149–155
28. Ricci C, Bloxham S, Kazarian SG (2007) J Cult Herit 8:387–395
29. Spring M, Ricci C, Peggie DA, Kazarian SG (2008) Anal Bioanal Chem 392:37–45
30. Cotte M, Checroun E, Mazel V, Solé VA, Richardin P, Taniguchi Y, Walter P, Susini J (2009) e-PS 6:1–9
31. Kazarian SG, Chan KLA (2006) Biochim Biophys Acta 1758:858–867
32. Fredericks P, Rintoul L, Coates J (2004) chap No. 7. In: Cazes J, Ewing GW (eds) Ewing's analytical instrumentation handbook. CRS Press, Boca Raton
33. Levin IW, Bhargava R (2005) Annu Rev Phys Chem 56:429–474
34. van der Weerd J, Heeren RMA, Boon JJ (2004) Stud Conserv 49:193–210
35. van Loon A, Keune K, Boon JJ (2005) In: Art'05—8th International Conference on the Non destructive Investigations and Microanalysis for the Diagnostic and Conservation of the Cultural and Environmental Heritage, Lecce
36. Lins A, Giannuzzi LA, Stevie FA, Price B, Tucker M, Gutman N (2001) MRS Proc 712:113–118
37. Boon JJ, Asahina S (2006) Microsc Microanal 12:1322–1323
38. Mazel V, Richardin P, Debois D, Touboul D, Cotte M, Brunelle A, Walter P, Laprévote O (2007) Anal Chem 79:9253–9260
39. Bruni S, Cariati F, Casadio F, Toniolo L (1999) Vib Spectrosc 20:15–25
40. van der Weerd J, Brammer H, Boon JJ, Heeren RMA (2002) Appl Spectrosc 56:276–283
41. Zieba-Palus J (1999) J Trace Microprobe Tech 17:299–308
42. Cotte M, Susini J, Solé VA, Taniguchi Y, Chillida J, Checroun E, Walter P (2008) J Anal At Spectrom 23:820–828
43. Gettens RJ, Kuhn H, Chase WT (1993) In: Roy A (ed) Artist's pigments: a handbook of their history and characteristics, vol 2. Oxford University Press, Oxford
44. Welcomme E, Walter P, Van Elslande E, Tsoucaris G (2006) Appl Phys A Mater Sci Process 83:551–556
45. Craddock PT (1996) In: Turner JS (ed) The dictionary of art. Grove's Dictionaries, New York
46. Lluveras A, Boularand S, Roqué J, Cotte M, Giráldez P, Vendrell-Saz M (2008) Appl Phys A 90:23–33
47. Thompson DV Jr (1954) Il libro dell'arte, the craftsman's handbook of Cennino d'Andrea Cennini. Dover, New York
48. Tintori L (1982) Burlington Mag 124:94–95
49. Cesareo R, Castellano A, Buccolieri G, Quarta S, Marabelli M, Santopadre P (2002) In: Van Grieken R, Janssens K, Van't dack L, Meersman G (eds) Art'02—7th International Conference on Non-destructive Testings and Microanalysis for the Diagnostics and Conservation of the Cultural and Environmental Heritage, Antwerp
50. Cesareo R, Castellano A, Buccolieri G, Quarta S, Marabelli M, Santopadre P (2004) Il Giornale delle Prove non distruttive Monitoraggio Diagnostica 3:66–72
51. Cesareo R, Castellano A, Buccolieri G, Quarta S, Marabelli M, Santopadre P, Gigante E, Ridolfi S (2005) In: van Grieken R, Janssens K (eds) Cultural heritage conservation and environmental impact assessment by non-destructive testing and micro-analysis. A.A. Balkema, London
52. Marabelli M, Santopadre P (2005) Bollettino d'arte volume speciale (Giotto nella Cappella degli Scrovegni): 121–144
53. Gettens RJ, Stout GL (1966) Painting materials. A short encyclopedia. Dover, New York